JACS
JOURNAL OF THE AMERICAN CHEMICAL SOCIETY

Article

pubs.acs.org/JACS

Halogen-Assisted Piezochromic Supramolecular Assemblies for Versatile Haptic Memory

Linyi Bai,[†] Purnandhu Bose,[†] Qiang Gao,[†] Yongxin Li,[†] Rakesh Ganguly,[†] and Yanli Zhao*[,†,‡]

[†]Division of Chemistry and Biological Chemistry, School of Physical and Mathematical Sciences, Nanyang Technological University, 21 Nanyang Link, Singapore 637371

[‡]School of Materials Science and Engineering, Nanyang Technological University, 50 Nanyang Avenue, Singapore 639798

Supporting Information

ABSTRACT: Sensory memory is capable of recording information and giving feedback based on external stimuli. Haptic memory in particular can retain the sensation of the interaction between the human body and the environment and help humans to describe the physical quantities in their environment and manipulate objects in daily activities. Although sensitive and accurate tactile sensors have been produced on optical and electronic devices, their rigorous operation and equipment requirements seriously limit their further applicability. In addition, their poor retainability after the removal of external stimuli also warrants further improvements. Thus, haptic memory materials, having simple structures and high sensitivity, are highly desired. Herein, we successfully developed two piezochromic assemblies assisted by halogen bonding for haptic memory. The halogen bond not only contributes to the fabrication of the network and enhances integrative stability but also broadens the natural piezofluorescent range, thus promoting sensory sensitivity. Moreover, the colorimetric change of the assemblies could be well-retained after the stimulus was removed. Upon mild heating treatment, the piezochromic response could be recovered to its original state, confirming the recyclability of this haptic memory material for use in practical applications. The present work enriches the library of piezochromic materials with enhanced performance for haptic memory.

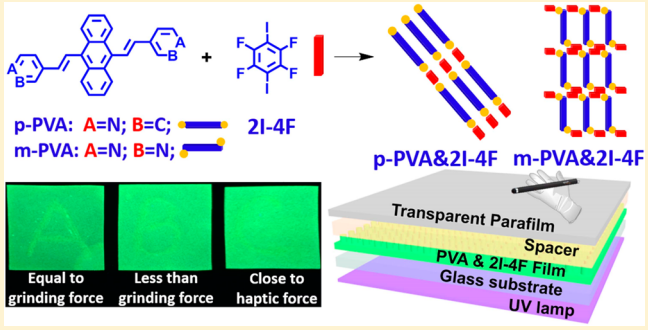

INTRODUCTION

Haptic memory is capable of retaining and conveying the impression of sensory details after the removal of external stimuli such as force, pain, shape, and texture; thus, any resulting incident can be exactly fed back and effectively manipulated.[1,2] Hence, sensory memory having a broad response range and accurate sensitivity is highly desired so that the information encoded in environmental stimuli can be clearly recorded and expressed.[3,4] To achieve this goal, some significant advancements have been witnessed over the past few years. For example, piezoelectric materials have been extensively investigated in bulk crystals, thin films, and nanostructures for pressure sensing, actuation, and harvesting.[5] In particular, a tremendous increase in sensitivity for tactile sensing based on micro- and nanostructures has been achieved.[6−9] Very recently, electronic skin devices have also been employed to emulate the exquisite tactile sensation of human skin.[10,11] However, the sensation information from these designs is not directly expressed but is fully dependent on the electric detector. This requirement limits the practical applications of these materials.

Visible piezochromic materials are a kind of smart material whose intrinsic color or fluorescence can be varied in response to external pressure stimuli on account of changes in the molecular packing mode.[12−14] It is highly desirable for such changes to be directly visualized by the naked eye while at the same time having simplified operation conditions and enabling the sensory information to be directly conveyed.[15,16] Undoubtedly, if these characteristics are combined with the superior sensitivity of piezoelectric materials, then detection using the obtained systems would be easily processed, thus providing valuable references for the development of future wearable technology. Recently, some exciting results in this field have been achieved, including the optimization of fluorescence properties[17,18] and the dynamic control of solid-state fluorescence with high reversibility and good reproducibility.[19−21] However, the narrow response range and low response efficiency of current haptic memory devices are still two key drawbacks, mainly because of the limited possibilities for altering the molecular structures of piezochromic materials.[22,23] Thus, developing novel strategies to solve this dilemma is an urgent task.

Herein, we introduce two halogen-bond-assisted supramolecular assemblies with piezochromic properties for haptic memory, in which two isomeric pyridylvinylanthracenes (p-

Received: October 27, 2016
Published: December 14, 2016

DOI: 10.1021/jacs.6b11057
J. Am. Chem. Soc. 2017, 139, 436−441

PVA and m-PVA; Figure 1a) are the key piezochromism-responsive molecules and the halogen bond is provided by tetrafluorodiiodobenzene (2I-4F). Owing to the strong electron-withdrawing effect of 2I-4F, charge transfer between 2I-4F and electron-rich pyridylvinylanthracenes occurs.[24−26] Assisted by halogen-bonding interactions between nitrogen atoms on pyridylvinylanthracenes and iodine atoms on 2I-4F, the self-assembled systems showed an effective enhancement in stability and strength.[27,28] More importantly, the utilization of 2I-4F broadens the colorimetric range and enables the response to be easily recognized. This unique feature could also be ascribed to the interaction between PVA and 2I-4F.[29]

The final molecular architectures were analyzed by single-crystal X-ray diffraction and scanning tunneling microscopy (STM). This preparation strategy not only promotes the stability and strength of the resulting assemblies but also enables the assemblies to possess a high sensory capacity and good sensitivity in response to pressure. Furthermore, the colorimetric change could be directly observed, which simplifies the detection conditions and facilitates the applicability of these materials. Interestingly, this response is reversible and could be recovered under mild heating treatment (60 °C for only 30 min), demonstrating the superior recyclability of these sensory assemblies.

RESULTS AND DISCUSSION

The halogen-bonding interaction used in this work is a remarkable noncovalent driving force and has been widely used in supramolecular assembly and crystal engineering.[30−33] Taking into consideration the presence of two pyridine groups in PVA molecules and two iodine atoms in 2I-4F, we mixed them in a 1:1 ratio to obtain co-crystals (p-PVA&2I-4F and m-PVA&2I-4F). Together with halogen bonding, intermolecular $\pi-\pi$ stacking and hydrogen bonding interactions resulted in the assembly of PVA and 2I-4F to form supramolecular complexes. The assembly modes between PVA and 2I-4F are proposed in Figure 1a, which mainly depend on halogen-bonding interactions involving halogen atom donors (2I-4F) and halogen atom acceptors (N in PVA) with the assistance of $\pi-\pi$ stacking interactions among these molecules.

The co-crystal structures further confirmed the above proposed modes. Single-crystal X-ray diffraction analyses of the two crystals clearly indicate their different assembly ratios and interactions. The p-PVA&2I-4F assembly crystallizes in triclinic space group $P\bar{1}$, with cell parameters of a = 8.11 Å, b = 10.12 Å, c = 10.58 Å, α = 116.79°, β = 106°, and γ = 92.45°, whereas m-PVA&2I-4F co-crystallizes into a monoclinic space group with cell parameters of a = 4.24 Å, b = 20.18 Å, c = 20.83 Å, α = 90°, β = 94.85°, and γ = 90°. For the assembly of p-PVA&2I-4F, the ratio of the two molecules in this complex is 1:1, in which each nitrogen atom of p-PVA complexes with an iodine atom (Figure 1b). For the assembly of m-PVA&2I-4F, however, the interacting ratio is 1:2, where each nitrogen atom of m-PVA complexes with only an iodine atom of a 2I-4F molecule and the other iodine is free (Figure 1c). Furthermore, the p-PVA&2I-4F complex is connected by a halogen bond between a nitrogen atom of p-PVA and an iodine atom of 2I-4F to form a linear assembly. The layer distance is 3.12 Å (Figure S1 in the Supporting Information), which is smaller than that of pure p-PVA crystals (layer distance 3.58 Å), implying the presence of strong $\pi-\pi$ stacking interactions in the assembly.[26] In sharp contrast, the m-PVA&2I-4F complex forms branched networks caused by the halogen-bonding interaction at an angle (Figure 1c), along with weak $\pi-\pi$ stacking interactions (layer distance 3.64 Å).[34] The different assembly modes were also verified by STM, where the assembly of p-PVA&2I-4F shows a linear structure, whereas m-PVA&2I-4F gives a network structure. Thus, different noncovalent interactions in these two types of assemblies play important roles.

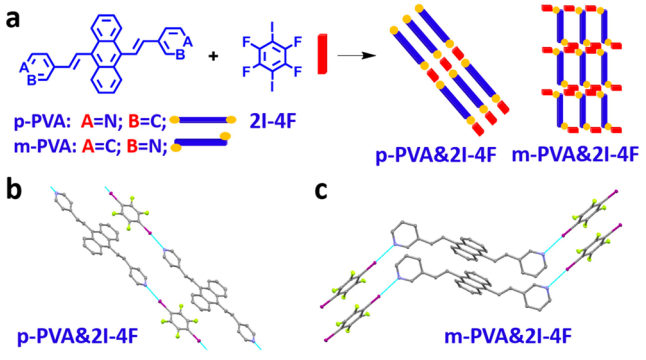

Figure 1. (a) Chemical structures of two piezochromic pyridylvinylanthracenes (p-PVA and m-PVA) and tetrafluorodiiodobenzene (2I-4F) as well as a schematic representation of their self-assembly process. (b, c) Intermolecular halogen-bonding interactions in co-crystals of p-PVA&2I-4F and m-PVA&2I-4F (CCDC numbers 1487910 and 1487911 contain the crystal details).

Next, morphological characterizations were performed using scanning electron microscopy (SEM), transmission electron microscopy (TEM), and powder X-ray diffraction (PXRD). As shown in Figure 2a−d, the SEM and TEM images clearly display the self-assembly of PVA and 2I-4F into regular rods with diameters of ∼200 nm and lengths of several micrometers, and these rods are uniformly distributed. High-resolution TEM images of p-PVA&2I-4F and m-PVA&2I-4F further suggest that the two types of assemblies are single crystalline in nature with clear crystal lattices.[35] Images of p-PVA&2I-4F exhibit d-spacing values of 6.3 and 3.1 Å, corresponding to the (001) and (010) planes, respectively. In contrast, the m-PVA&2I-4F crystal grows along the (010) plane with the lowest attachment energy and then expands along the (100) direction. In its XRD pattern (Figure 2e), there is a sharp peak at 5.63°, indicating that such an assembly mode leads to a porous network architecture.

To understand the stacking modes of these two assemblies, both Chem3D and Materials Studio software with the growth morphology algorithm were used to simulate and analyze the intermolecular interactions during the self-assembly. The calculation results depicted in Figures S1 and S2 reveal the size of each molecule and the stacking mode in the assemblies. p-PVA&2I-4F may grow along the (100) axis, and the location of the lowest contact energy in the (001) direction (Figure S2a) implies that it predominates in the morphology of the assembly.[36] In comparison, m-PVA&2I-4F may grow into networks (Figure S2b), and among its predicted crystal planes, (100), (010), and (001) may be dominant in the resulting bulk crystals.[26,37] This prediction is consistent with the corresponding crystal diffraction results.

These results indicate that different noncovalent interactions between PVA and 2I-4F could lead to different assemblies with distinct molecular packing modes. After carefully analyzing the packing modes, we explored the optical properties of PVA molecules and their assemblies with 2I-4F. UV absorbance and fluorescence measurements (Figure 2f,g) were first conducted.

DOI: 10.1021/jacs.6b11057
J. Am. Chem. Soc. 2017, 139, 436−441

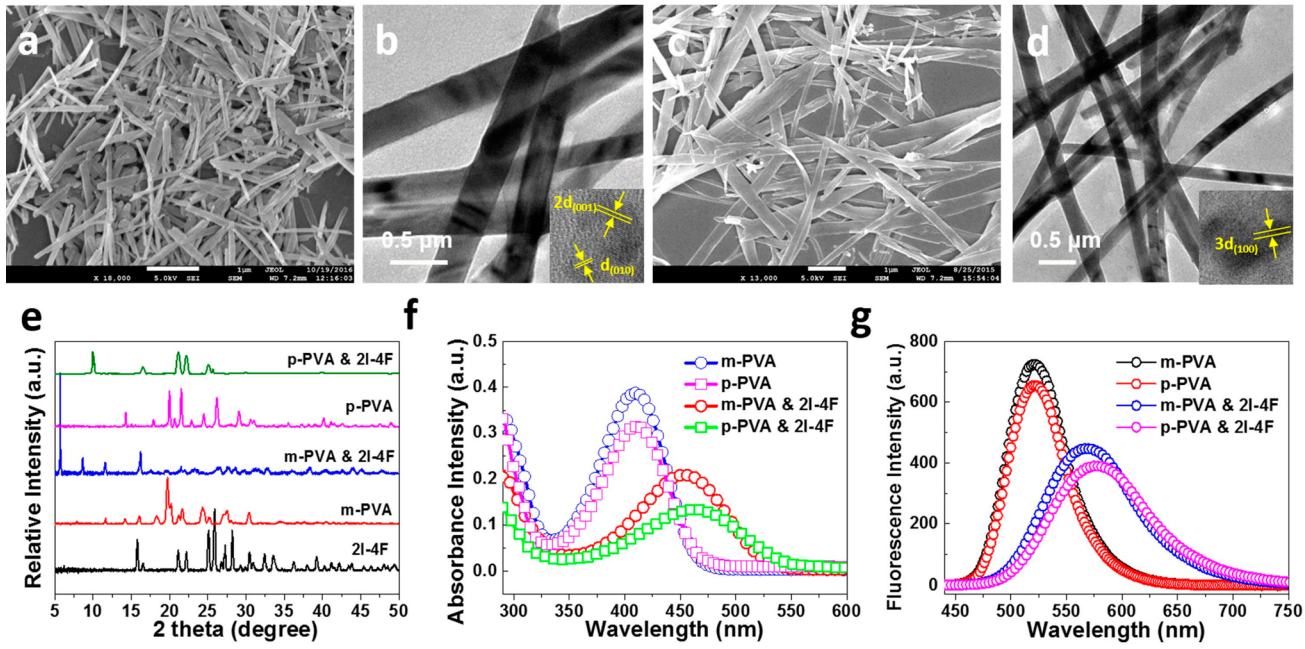

Figure 2. SEM and TEM images of (a, b) p-PVA&2I-4F and (c, d) m-PVA&2I-4F assemblies. Insets in the TEM images (b, d) are high-resolution TEM images of the two assemblies. (e) PXRD patterns of the two assemblies and corresponding starting materials, i.e., 2I-4F, m-PVA, and p-PVA. (f, g) UV absorbance and fluorescence spectra of m-PVA and p-PVA as well as p-PVA&2I-4F and m-PVA&2I-4F assemblies.

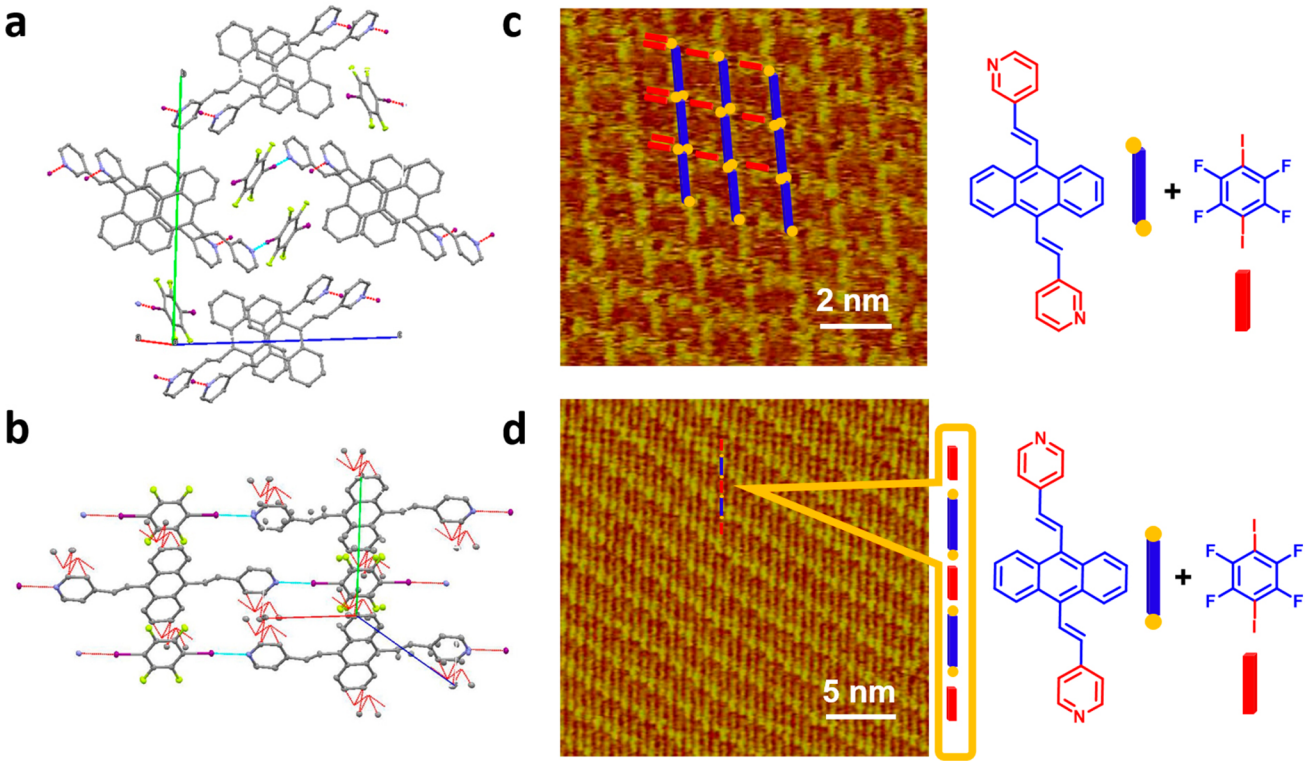

Figure 3. Single-crystal packing structures of (a) m-PVA&2I-4F and (b) p-PVA&2I-4F, where iodine and fluorine are colored yellow-green and pink, respectively, and the PVA backbone is colored gray. High-resolution STM image of the two assemblies: (c) m-PVA&2I-4F and (d) p-PVA&2I-4F. Tunneling conditions: V_{bias} = 742 mV, I_t = 460 pA.

Interestingly, the designed assemblies performed as expected, where PVA molecules were utilized as the main luminescent piezochromic unit to respond to external pressure and 2I-4F was incorporated to extend the piezochromic range via the charge transfer effect caused by its strong electron-pulling effect, resulting in the piezochromic change becoming much more prominent. In the UV absorption spectra (Figure 2f), significant red shifts (from 407 to 451 nm for the m-PVA&2I-4F assembly and from 411 to 458 nm for the p-PVA&2I-4F assembly) could be observed after formation of the assemblies, and the full width at half-maximum (fwhm) also became larger. Such changes could be attributed to the interactions between

DOI: 10.1021/jacs.6b11057
J. Am. Chem. Soc. 2017, 139, 436−441

PVA and 2I-4F.[38] The fluorescence spectra (Figure 2g) also broadened, showing a red shift from 529 nm (green) to ~570 nm (yellow green) after the formation of these two assemblies. Such a red shift in the luminescence makes the emission of these assemblies close to the relatively narrow range of yellow emission, which is beneficial for the subsequent piezochromic response, particularly with regard to sensitivity.[39,40]

To better understand the relationship between the assembly mode and physical properties of these materials, we investigated their assembly modes using STM with their single crystal structures as references (Figure 3a,b). For the assembly of m-PVA and 2I-4F, we observed an ordered and porous network structure, as shown in Figure 3c, where the bright rods and the junction points could be easily recognized. This binary system with a 2:1 molecular ratio between m-PVA and 2I-4F first forms a trilateral shape on account of the angle of the halogen-bonding interaction and then results in a tetragonal porous structure via intermolecular interactions. We measured the length of these rods and compared it with the calculated value. The length of the longitudinal rod is 1.5 ± 0.1 nm, and the length of the lateral rod is ~0.7 nm, which match well with theoretically calculated lengths of the two molecules (m-PVA 1.49 nm and 2I-4F 0.7 nm; Figure S2). Having the 2:1 interaction ratio, the assembled structure was proposed as in Figure 3c. Interestingly, the pore size of the network structure is ~1.6 nm, very close to the calculated value based on the PXRD pattern (2θ = 5.57°, d = 1.58 nm; Figure 2e). For the p-PVA&2I-4F assembly, the p-PVA molecule interacts with 2I-4F via the two pyridyl groups to form a binary linear structure and finally self-assembles into a long linear superstructure (Figure 3d), in which thick rods and short spots could be clearly observed. With the help of high-resolution STM images, the thick and bright rods are ascribed to p-PVA, and the short and dark spots are attributed to 2I-4F. The dark spots were measured to be 0.7 ± 0.1 nm long, in agreement with the length of the 2I-4F molecule. One p-PVA molecule is attached to two 2I-4F molecules in a head-to-head fashion to form the linear structure. The iodine atoms in 2I-4F and the pyridyl groups in p-PVA interact closely with each other through the C−N···I halogen-bonding interaction with an angular arrangement close to 180°.

A remaining question is whether such assembled structures, i.e., linear stacking and network, could impart any unique properties to the two assemblies. To address this query, several physical property characterizations, including thermal stability, composition, and pore size distributions, were performed (Figures S3−S5). In terms of pore size, a remarkable difference in the surface areas of the two assemblies was exhibited (919 m^2/g for m-PVA&2I-4F and 143 m^2/g for p-PVA&2I-4F). Furthermore, the pore size distributions of the two assemblies also match well with the above STM observations, in which m-PVA&2I-4F has a main pore diameter of ~15 Å, whereas p-PVA&2I-4F is ~2.5 Å, indicating their distinct styles of assembly.

Upon obtaining the structural information, the solid-state emission of the two assemblies and their piezochromic properties were carefully explored by examining their fluorescence. As shown in Figure 4, powdered forms of the two assemblies exhibit a noticeable luminescence color change under a relatively low pressure treatment compared with the corresponding nonassembled PVA powder (Figure S6). Owing to the charge transfer effect, the two assemblies showed strong green emission at λ_{max} ~ 560 nm. After grinding the two

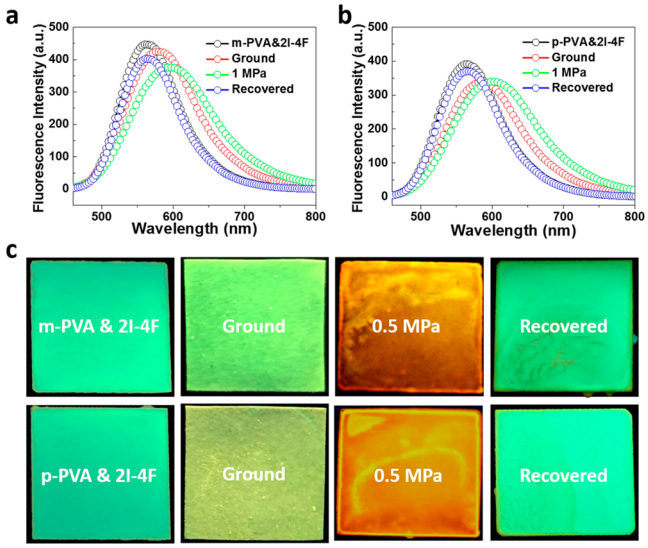

Figure 4. (a, b) Fluorescence spectra of the two assemblies on a glass substrate under excitation at 450 nm in response to different pressure treatments as well as their recovery spectra. (c) Practical fluorescence images of the two assemblies under excitation at 365 nm after different pressure treatments.

assemblies with a pestle and pressing them, their powders presented a red shift with yellow emission (λ_{max} = 578 nm) under the irradiation of 365 nm UV light. After being heated at around 60 °C for 30 min, the two ground powders recovered their initial green emission (λ_{max} ~ 560 ± 1 nm; Figure 4c). The interconversion of the two states with their different emission color changes was fully reversible by grinding and heating processes. The red shift of 18 nm in the fluorescence emission of the two assemblies upon grinding and the recovery of the fluorescence emission to the initial state under heating are attributed to their remarkable piezochromic effect.

This recovery process was subsequently analyzed via PXRD (Figure S7), where a comparison among the initial assembled state, that after pressure stimuli, and that upon heating treatment was performed. Obviously, new peaks such as 2θ ~ 27.5° and ~38.6° for the two assemblies appeared after 1 MPa pressure was applied, indicating that stacking structural changes resulted from the pressure stimuli. Then, a mild heating treatment (60 °C for 30 min) enabled these changed assemblies to recover to their initial states. Although we attempted to further analyze the structural changes upon applying pressure stimuli, their crystals were unfortunately destroyed by the pressure treatment.

Next, we studied the piezochromic behavior, where the treatment pressure was enhanced from 0.25 MPa (equivalent to grinding) to 1 MPa to cover the whole range of a haptic sensor, and we recorded the fluorescence changes of the two assemblies in the solid state. As the applied pressure increased, the fluorescence emission of the two assemblies exhibited more noticeable red shifts as compared with those from the grinding cases (Figure 4a,b). The observed fluorescent color change from green (561 nm) to orange-red (602 nm) is probably the most sensitive piezochromic shift under such low pressure treatment reported to date.[19] Additionally, we also performed a series of comparative experiments (Figures S8−S10), where the fluorescent spectra with λ_{max} = 582 nm at an applied pressure of 0.25 MPa were very similar to that of the powders ground with a pestle. An enhanced applied pressure of 1 MPa led to a

DOI: 10.1021/jacs.6b11057
J. Am. Chem. Soc. 2017, 139, 436−441

luminescence change to redder emission with λ_{max} = 602 nm. Obviously, the grinding method is not powerful enough to give rise to a strong piezochromic effect. According to previous reports,[38,41] it is believed that dramatic changes in the luminescence color of assembly powders under applied pressures are the result of changes in their molecular assemblies. Then, we performed an annealing treatment to recover the emission, in which the changes in the wavelength of solid-state emission could be repeated many times, suggesting that the reversibility is excellent for use in cycling processes. Noticeably, both emission and absorption of these two molecular assemblies were completely reversible under alternating heating and pressing (or grinding) treatments, and this feature of reversible color change makes them promising candidates as optical recording and temperature/pressure-sensing systems.

To verify the application potential of these materials as pressure-sensing systems, a haptic memory device was built as shown in Figure 5a, which consists of a UV lamp as the excitation source, a glass substrate, a PVA&2I-4F assembly film, and a transparent layer of parafilm on top of the assembly film for protection. In this way, writing with pressure treatment was successfully visualized (Figure 5b). Upon pressing simply with a metal spatula or glass rod, the touched area immediately changed its emission color, which was similar to the case of grinding in the solid-state fluorescent studies. As shown in Figure 5b, three letters, ABC, were generated by pressing the device with different strengths (equal to grinding force, less than grinding force, and close to haptic force). Clear changes (letter A) were observed with a treatment equivalent to the grinding force. Interestingly, this change could be observed only under a UV lamp, and the fluorescent color change occurs only at the areas that is pressed. The rest remains in its original fluorescent state, indicating the promising potential of such materials for anti-fake fluorescence recording, in addition to piezochromic sensors. In order to show the recyclability of the device, recovery experiments were performed with a similar procedure to the heating of the powder samples (heating at 60 °C for 30 min), and the device could be recovered to its original state for reuse. This property indicates that the sensing memory device is capable of retaining tactile information after external pressure and regaining its original state under a recovery process.

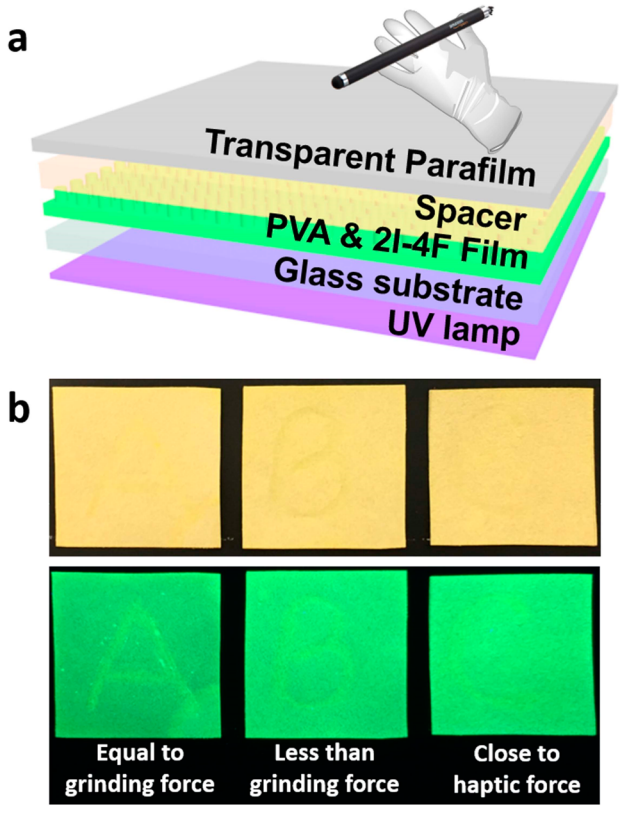

Figure 5. (a) Schematic representation of the haptic memory device, comprising a transparent parafilm, PVA&2I-4F film, glass substrate, and UV lamp. (b) Practical fluorescence images (letters A, B, and C from left to right) of the haptic memory device under excitation at 365 nm after touch drawing.

CONCLUSIONS

In summary, we have successfully developed two piezochromic assemblies from PVA and 2I-4F via halogen bonding and $\pi-\pi$ stacking interactions. On the basis of slight differences in the backbones of the two PVA molecules, two different assembly structures were achieved, i.e., linear wires and networks. The as-synthesized assemblies effectively broadened the original piezochromic range on account of the charge transfer effect among these molecules, enabling the response to be more sensitive and obvious. In a study of their touch memory performance, the two assemblies exhibited significant piezochromic behavior with color changes in response to different external pressures. Interestingly, such changes could be well recovered under mild heating at 60 °C, indicating their great potential for applications in practical devices. The present supramolecular assemblies with unique features such as high sensitivity and easy handling provide excellent references for further design and preparation of sensing systems through noncovalent bonding strategies. Overall, these two piezochromic assemblies with enhanced response performance may open up a rational approach for developing a broad class of novel functional materials with desired shapes and photophysical functions.

EXPERIMENTAL SECTION

Synthesis of PVA. PVA molecules were synthesized from compounds i and ii, which can be found in the Supporting Information. Compound ii (0.5 g, 1.0 mmol) was stirred with *n*-BuLi (2M, 2.0 mL, 4.0 mmol) in anhydrous THF (50 mL) under nitrogen. A solution of formylpyridine (0.25 mL, 2.5 mmol) in THF (50 mL) was added to the solution in an ice bath, and the mixture was stirred at room temperature overnight. 4-Formylpyridine was used for the synthesis of p-PVA, and 3-formylpyridine was used for m-PVA. The resultant precipitate was washed successively with MeOH to give the final compounds as yellow powders in ~45% yields.

p-PVA. ^{1}H NMR (400 MHz, $CDCl_3$) δ 8.70 (dd, J = 4.6, 1.5 Hz, 4H), 8.33 (dd, J = 6.8, 3.3 Hz, 4H), 8.16 (d, J = 16.4 Hz, 2H), 7.54 (dd, J = 4.8, 1.7 Hz, 4H), 7.53−7.49 (m, 4H), 6.90 (d, J = 16.5 Hz, 2H); ^{13}C NMR (101 MHz, $CDCl_3$) δ 150.49 (s), 144.24 (s), 135.28 (s), 132.08 (s), 129.92 (s), 129.39 (s), 126.15 (s), 125.80 (s), 120.97 (s); HRMS calcd for $C_{28}H_{20}N_2$, 385.1705; found, 385.1722.

m-PVA. ^{1}H NMR (400 MHz, $CDCl_3$) δ 8.88 (s, 1H), 8.60 (s, 1H), 8.36 (dd, J = 7.9, 4.6 Hz, 2H), 8.01 (t, J = 13.3 Hz, 2H), 7.51 (dd, J = 6.9, 3.2 Hz, 2H), 7.40 (dd, J = 7.9, 4.8 Hz, 1H), 6.93 (d, J = 16.6 Hz, 1H); ^{13}C NMR (101 MHz, $CDCl_3$) δ 149.12 (s), 148.58 (s), 134.01 (s), 132.87 (d, J = 11.5 Hz), 132.32 (s), 129.48 (s), 127.44 (s), 126.25 (s), 125.61 (s), 123.72 (s); HRMS calcd for $C_{28}H_{20}N_2$, 385.1705; found, 385.1714.

DOI: 10.1021/jacs.6b11057
J. Am. Chem. Soc. 2017, 139, 436−441

Crystal Growth of the Two Assemblies. In a typical experiment, PVA and 2I-4F were dissolved in chloroform in a 1:1 molar ratio. The slow evaporation of the chloroform solution resulted in several needle-shaped yellow crystals.

Piezofluorescent Performance of the Two Assemblies. Powders of the assemblies were placed in the holes (diameter 200 mm) of a T301 steel gasket. A small chip was inserted into the samples for in situ pressure calibration. A mixture solution of methanol and ethanol (4:1) was employed as a pressure-transmitting medium. The pressure on the samples was determined by measuring the separation and width of the defined lines. The fluorescence measurement at high pressure was carried out at room temperature.

Recovery of the Two Assemblies after Pressure Treatment. Recovery of the assemblies to their initial state relies on a heat treatment, in which fluorescence-changed PVA&2I-4F powders were placed in an oven at 60 °C for 30 min. A comparative experiment in which PVA&2I-4F powders were directly placed on a hot plate was also performed. The recovery of the fluorescence was more effective under the former conditions than in the latter case.

■ ASSOCIATED CONTENT

Supporting Information

The Supporting Information is available free of charge on the ACS Publications website at DOI: 10.1021/jacs.6b11057.

Synthetic details of PVA molecules; property characterizations; and TGA, FTIR, XPS, and crystal data (PDF)
m-PVA&2I-4F crystallographic data (CIF)
p-PVA&2I-4F crystallographic data (CIF)

■ AUTHOR INFORMATION

Corresponding Author

*zhaoyanli@ntu.edu.sg

ORCID

Yanli Zhao: 0000-0002-9231-8360

Notes

The authors declare no competing financial interest.

■ ACKNOWLEDGMENTS

This work was financially supported by the Singapore Academic Research Fund (RG112/15 and RG19/16).

■ REFERENCES

(1) Lucarotti, C.; Oddo, C. M.; Vitiello, N.; Carrozza, M. C. *Sensors* **2013**, *13*, 1435−1466.
(2) Zhu, B.; Wang, H.; Liu, Y.; Qi, D.; Liu, Z.; Wang, H.; Yu, J.; Sherburne, M.; Wang, Z.; Chen, X. *Adv. Mater.* **2016**, *28*, 1559−1566.
(3) Pasternak, T.; Greenlee, M. W. *Nat. Rev. Neurosci.* **2005**, *6*, 97−107.
(4) Stuart, M. A. C.; Huck, W. T. S.; Genzer, J.; Muller, M.; Ober, C.; Stamm, M.; Sukhorukov, G. B.; Szleifer, I.; Tsukruk, V. V.; Urban, M.; Winnik, F.; Zauscher, S.; Luzinov, I.; Minko, S. *Nat. Mater.* **2010**, *9*, 101−113.
(5) Pan, C.; Chen, M.; Yu, R.; Yang, Q.; Hu, Y.; Zhang, Y.; Wang, Z. L. *Adv. Mater.* **2016**, *28*, 1535−1552.
(6) Gong, S.; Schwalb, W.; Wang, Y. W.; Chen, Y.; Tang, Y.; Si, J.; Shirinzadeh, B.; Cheng, W. L. *Nat. Commun.* **2014**, *5*, 3132.
(7) Mannsfeld, S. C. B.; Tee, B. C. K.; Stoltenberg, R. M.; Chen, C.; Barman, S.; Muir, B. V. O.; Sokolov, A. N.; Reese, C.; Bao, Z. N. *Nat. Mater.* **2010**, *9*, 859−864.
(8) Pang, C.; Lee, G. Y.; Kim, T. I.; Kim, S. M.; Kim, H. N.; Ahn, S. H.; Suh, K. Y. *Nat. Mater.* **2012**, *11*, 795−801.
(9) Someya, T.; Kato, Y.; Sekitani, T.; Iba, S.; Noguchi, Y.; Murase, Y.; Kawaguchi, H.; Sakurai, T. *Proc. Natl. Acad. Sci. U. S. A.* **2005**, *102*, 12321−12325.
(10) Wang, X. W.; Gu, Y.; Xiong, Z. P.; Cui, Z.; Zhang, T. *Adv. Mater.* **2014**, *26*, 1336−1342.
(11) Xue, X.; Fu, Y.; Wang, Q.; Xing, L.; Zhang, Y. *Adv. Funct. Mater.* **2016**, *26*, 3128−3138.
(12) Nagura, K.; Saito, S.; Yusa, H.; Yamawaki, H.; Fujihisa, H.; Sato, H.; Shimoikeda, Y.; Yamaguchi, S. *J. Am. Chem. Soc.* **2013**, *135*, 10322−10325.
(13) Sagara, Y.; Komatsu, T.; Ueno, T.; Hanaoka, K.; Kato, T.; Nagano, T. *J. Am. Chem. Soc.* **2014**, *136*, 4273−4280.
(14) Sagara, Y.; Mutai, T.; Yoshikawa, I.; Araki, K. *J. Am. Chem. Soc.* **2007**, *129*, 1520−1521.
(15) Dong, Y. Q.; Lam, J. W. Y.; Tang, B. Z. *J. Phys. Chem. Lett.* **2015**, *6*, 3429−3436.
(16) Zhang, X.; Chi, Z.; Zhang, J.; Li, H.; Xu, B.; Li, X.; Liu, S.; Zhang, Y.; Xu, J. *J. Phys. Chem. B* **2011**, *115*, 7606−7611.
(17) Benito, Q.; Le Goff, X. F.; Maron, S.; Fargues, A.; Garcia, A.; Martineau, C.; Taulelle, F.; Kahlal, S.; Gacoin, T.; Boilot, J.-P.; Perruchas, S. *J. Am. Chem. Soc.* **2014**, *136*, 11311−11320.
(18) Yoon, S.-J.; Chung, J. W.; Gierschner, J.; Kim, K. S.; Choi, M.-G.; Kim, D.; Park, S. Y. *J. Am. Chem. Soc.* **2010**, *132*, 13675−13683.
(19) Dong, Y.; Xu, B.; Zhang, J.; Tan, X.; Wang, L.; Chen, J.; Lv, H.; Wen, S.; Li, B.; Ye, L.; Zou, B.; Tian, W. *Angew. Chem.* **2012**, *124*, 10940−10943.
(20) Wang, J.; Mei, J.; Hu, R.; Sun, J. Z.; Qin, A.; Tang, B. Z. *J. Am. Chem. Soc.* **2012**, *134*, 9956−9966.
(21) Yagai, S.; Seki, T.; Aonuma, H.; Kawaguchi, K.; Karatsu, T.; Okura, T.; Sakon, A.; Uekusa, H.; Ito, H. *Chem. Mater.* **2016**, *28*, 234−241.
(22) Ma, Z.; Wang, Z.; Meng, X.; Ma, Z.; Xu, Z.; Ma, Y.; Jia, X. *Angew. Chem.* **2016**, *128*, 529−532.
(23) Toma, O.; Allain, M.; Meinardi, F.; Forni, A.; Botta, C.; Mercier, N. *Angew. Chem., Int. Ed.* **2016**, *55*, 7998.
(24) Das, A.; Ghosh, S. *Angew. Chem., Int. Ed.* **2014**, *53*, 2038−2054.
(25) Kumar, M.; Venkata Rao, K.; George, S. J. *Phys. Chem. Chem. Phys.* **2014**, *16*, 1300−1313.
(26) Zhu, W.; Zheng, R.; Zhen, Y.; Yu, Z.; Dong, H.; Fu, H.; Shi, Q.; Hu, W. *J. Am. Chem. Soc.* **2015**, *137*, 11038−11046.
(27) Lucassen, A. C. B.; Karton, A.; Leitus, G.; Shimon, L. J. W.; Martin, J. M. L.; van der Boom, M. E. *Cryst. Growth Des.* **2007**, *7*, 386−392.
(28) Walsh, R. B.; Padgett, C. W.; Metrangolo, P.; Resnati, G.; Hanks, T. W.; Pennington, W. T. *Cryst. Growth Des.* **2001**, *1*, 165−175.
(29) Bai, L.; Wang, P.; Bose, P.; Li, P.; Zou, R.; Zhao, Y. *ACS Appl. Mater. Interfaces* **2015**, *7*, 5056−5060.
(30) Metrangolo, P.; Neukirch, H.; Pilati, T.; Resnati, G. *Acc. Chem. Res.* **2005**, *38*, 386−395.
(31) Erdelyi, M. *Chem. Soc. Rev.* **2012**, *41*, 3547−3557.
(32) Li, B.; Zang, S.-Q.; Wang, L.-Y.; Mak, T. C. W. *Coord. Chem. Rev.* **2016**, *308* (Part 1), 1−21.
(33) Politzer, P.; Lane, P.; Concha, M. C.; Ma, Y.; Murray, J. S. *J. Mol. Model.* **2007**, *13*, 305−311.
(34) Zheng, Q.-N.; Liu, X.-H.; Chen, T.; Yan, H.-J.; Cook, T.; Wang, D.; Stang, P. J.; Wan, L.-J. *J. Am. Chem. Soc.* **2015**, *137*, 6128−6131.
(35) Zhu, W.; Dong, H.; Zhen, Y.; Hu, W. *Sci. China Mater.* **2015**, *58*, 854−859.
(36) Zhang, H. Y.; Zhang, Z. L.; Ye, K. Q.; Zhang, J. Y.; Wang, Y. *Adv. Mater.* **2006**, *18*, 2369−2372.
(37) Yoon, S. J.; Chung, J. W.; Gierschner, J.; Kim, K. S.; Choi, M. G.; Kim, D.; Park, S. Y. *J. Am. Chem. Soc.* **2010**, *132*, 13675−13683.
(38) Li, S.; Lin, Y.; Yan, D. *J. Mater. Chem. C* **2016**, *4*, 2527−2534.
(39) Maclean, M.; MacGregor, S. J.; Anderson, J. G.; Woolsey, G. *FEMS Microbiol. Lett.* **2008**, *285*, 227−232.
(40) Costa-Fernández, J. M.; Pereiro, R.; Sanz-Medel, A. *TrAC, Trends Anal. Chem.* **2006**, *25*, 207−218.
(41) Sun, J.-K.; Chen, C.; Cai, L.-X.; Ren, C.-X.; Tan, B.; Zhang, J. *Chem. Commun.* **2014**, *50*, 15956−15959.

DOI: 10.1021/jacs.6b11057
J. Am. Chem. Soc. 2017, 139, 436−441